



HAL
open science

Impact of Alkali-Silica Reaction and Delayed Ettringite Formation-induced cracking on air permeability and water diffusivity in concrete

Joe Maalouf, Hugo Gérard Jacques Cagnon, Jérôme Verdier, Stéphane Multon, Jacques Jabbour, David Bouhjiti

► To cite this version:

Joe Maalouf, Hugo Gérard Jacques Cagnon, Jérôme Verdier, Stéphane Multon, Jacques Jabbour, et al.. Impact of Alkali-Silica Reaction and Delayed Ettringite Formation-induced cracking on air permeability and water diffusivity in concrete. *Case Studies in Construction Materials*, 2025, 22, pp.e04183. 10.1016/j.cscm.2024.e04183 . hal-04871079v2

HAL Id: hal-04871079

<https://hal.science/hal-04871079v2>

Submitted on 17 Jan 2025

HAL is a multi-disciplinary open access archive for the deposit and dissemination of scientific research documents, whether they are published or not. The documents may come from teaching and research institutions in France or abroad, or from public or private research centers.

L'archive ouverte pluridisciplinaire **HAL**, est destinée au dépôt et à la diffusion de documents scientifiques de niveau recherche, publiés ou non, émanant des établissements d'enseignement et de recherche français ou étrangers, des laboratoires publics ou privés.



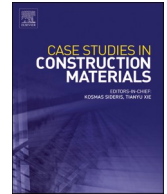
Distributed under a Creative Commons Attribution 4.0 International License



ELSEVIER

Contents lists available at ScienceDirect

Case Studies in Construction Materials

journal homepage: www.elsevier.com/locate/cscm

Impact of alkali-silica reaction and delayed ettringite formation-induced cracking on air permeability and water diffusivity in concrete

Joe Maalouf^a, Hugo Cagnon^{a,*}, Jérôme Verdier^a, Stéphane Multon^a, Jacques Jabbour^b, David Bouhjiti^b

^a University of Toulouse; UPS, INSA; LMDC (Laboratoire Matériaux et Durabilité des Constructions), 135, avenue de Rangueil, Toulouse Cedex 04, F-31 077, France

^b Institute of radioprotection and nuclear safety, IRSN/PSN-EXP/SES/LMAPS, Fontenay-aux-Roses 92260, France

ARTICLE INFO

Keywords:

Alkali-silica reaction
Delayed ettringite formation
Transport properties
Diffusivity
Permeability
Cracking

ABSTRACT

Managing the effects of Internal Swelling Reactions (ISR), Delayed Ettringite Formation (DEF), and Alkali-Silica Reaction (ASR) on the integrity of concrete structures with containment functions, such as nuclear facilities and dams, remains a major challenge for both long-term operation and maintenance. However, the effect of cracking caused by ISR on the mass transport properties of concrete has not been extensively investigated. To date, there is limited characterization of water diffusive phenomena and permeability in concretes affected by ISR. To address these gaps, a comprehensive and complete characterization of mass transport properties evaluating water porosity, pore distribution, diffusivity, and apparent air permeability in concrete affected by ASR and DEF is conducted hereafter. This experimental work points out the impact of cracking induced by expansion on these parameters. Water diffusivity is multiplied by a maximum of 2.8 for 0.22 % expansion in DEF, while permeability can be multiplied by 44 for ASR concrete after expansion to 0.22 %. The cracking patterns induced by ASR and DEF are different, leading to differences in the evolution of transport properties. Overall, crucial experimental insights to enhance existing models are thus highlighted, particularly concerning the intricate relationship between expansion advancement, cracking, and mass transport properties in concrete.

1. Introduction

Internal swelling reactions (ISR) such as Alkali-Silica Reaction (ASR) and Delayed Ettringite Formation (DEF) develop slowly over years and jeopardize structural integrity over decades. ISR cause concrete expansion and reduce its mechanical strength [1–4]. ISR also alter the transport properties of damaged concrete by affecting the porosity network but this impact is little documented in the literature. In sound concrete, permeability is low and fluid flows through the cementitious matrix pores according to a given connectivity network [5]. As concrete often cracks in structures due to various thermo-hydro-mechanical loads, permeability increases which makes the quantification of cracking effects on durability crucial [6–8]. Indeed, cracks create pathways for aggressive agents by aqueous or air transport and, when sufficiently developed, increase the leakage rates in containment structures [9]. With that regard,

* Corresponding author.

E-mail address: cagnon@insa-toulouse.fr (H. Cagnon).

<https://doi.org/10.1016/j.cscm.2024.e04183>

Received 18 September 2024; Received in revised form 12 December 2024; Accepted 28 December 2024

Available online 30 December 2024

2214-5095/© 2025 The Authors. Published by Elsevier Ltd. This is an open access article under the CC BY license (<http://creativecommons.org/licenses/by/4.0/>).

cracks also create a favourable environment for the penetration of water which is an essential element for ASR and DEF [7,6,10–12]. Concrete is a porous material, which underscores the importance of transport properties with very practical implications for water and ionic diffusivity, as well as air and water permeability. These transport properties are related to open porosity, but also to pore size and less easily measured properties such as constriction and tortuosity, which can be inferred by inverse analysis of the properties measured on concrete specimens. In cracked concrete damaged by ISR, there is a combination of two porous networks: the initial network formed by the combination of porosity in the cement paste and the interfacial transition zones (highly porous interface between cement paste and aggregate), and the network created by the cracks due to ISR. It is therefore essential for the containment manager to characterize each of these networks and the effect of their coupling.

The evolution of the mechanical properties of concrete damaged by ASR and DEF has been well-studied in the literature [13–21]. The impact of cracks induced by mechanical loading on the permeability of concrete has also been highlighted in several studies in the literature [9,22–28], but mainly for concrete in dry state without evaluation of the impact of the saturation. However, few studies examine ASR and DEF effects on transport properties. As the morphology of cracks induced by ISR is very different from cracks induced by mechanical loading, specific studies are necessary. The evolution of chloride diffusion with ASR [29] and air permeability in standard conditions (after drying at 105 °C) with DEF [13,30,31] have been studied. But, for structures that may be affected by ISR and whose primary function is to ensure containment or waterproofing, the evaluation of air permeability for different saturation rates is crucial [32–35]. In fact, most structures have concrete saturation rates between 50 and 100 %. The core of massive structures and locations exposed to rainfall are typically highly saturated (over 80 % at 50 mm depth) [36–38]. Even under normal dry conditions, the saturation of most structural concrete is between 50 and 60 %. Since water diffusivity and air permeability are strongly influenced by the saturation rate, it is necessary to evaluate their evolution with ISR cracking under realistic conditions and thus for common saturation rates of structures. Currently, no data are available to evaluate the air leakage in structures damaged by ISR under real environmental conditions. The experimental work presented in this paper is a first attempt to provide and analyze the data necessary to quantify the evolution of the containment properties of structural concrete damaged by ASR or DEF.

The differences in physicochemical mechanisms underlying ASR and DEF can lead to different patterns of cracking (variation of the extent, the distribution, the location, the opening, etc.) [3,39,40]. Moreover, ASR, DEF, and freeze-thaw (FT) cycles, both individually and in combination was found to correlate well with expansion levels and provided reliable assessments regardless of the extent of deterioration. Notably, FT and DEF exhibited higher DRI values than ASR at low and intermediate expansion levels due to the early formation of opened cracks in the cement paste. Combined mechanisms, particularly ASR + FT, proved to be more damaging [41]. However, FT occurs primarily in the skin of concrete structures. In fact, negative temperatures can hardly reach the core of solid containment structures, unlike ASR and DEF, which develop throughout the depth of the wall.

Accordingly, ASR and DEF may impact transport properties differently as new phases from ASR and DEF may fill the induced cracks. Finally, this study aims at quantifying the effect of ASR and DEF expansion on transport properties and addresses the issue as following. First, water porosity and mercury porosimetry are analyzed with a special focus on the average radius to characterize the porous network opening. Second, the drying kinetics are investigated to assess the water diffusivity. Third, apparent air permeability is evaluated at various saturation rates for expansion levels. Permeability can serve as an indicator of the effects of the pore network and cracking due to chemical expansion. A detailed characterization of the transport properties in concrete affected by ASR or DEF for different saturation rates and expansion levels has not been extensively performed. This complete characterization of the transport properties of damaged concrete is necessary to develop accurate micro- and mesoscopic scale models. Models combining mass transport in normal porosity and cracking due to ISR in high saturation conditions are needed to predict the evolution of transport properties in such damaged concrete and to predict both its performance and future life.

The data obtained in this study can be used to propose empirical laws for macro models or to test the ability of micro or mesoscopic models to evaluate transport properties in concrete affected by ISR. The database generated by this study can also support the development of machine learning models that require a large amount of data. In this work, only the effect of cracking due to ASR or DEF in the absence of any extrinsic mechanical loading is of interest.

2. Materials and methods

The samples are cylindrical, 30 cm high and 15 cm in diameter, and were first used for expansion measurements. When the targeted expansion was reached, they were cut into 5 cm thick slices for permeability measurements. Unless otherwise noted, three samples are

Table 1

Concrete mix proportions for control concrete, ASR and DEF, W/C = 0.56 based on [13,30,42].

Constituents [kg/m ³]	ASR	DEF Control Concrete
Cement CEM II A-LL 42,5 R CE PM-CP2 NF	350	
Limestone sand 0/4	772	
Limestone aggregate 4/11,2	-	316
Limestone aggregate 11,2/22,4	-	784
Siliceous-limestone aggregate PR 4/14	316	-
Siliceous-limestone aggregate PR 14/20	784	-
Efficient water	195	
Superplasticizer	-	1.225 (0.35 %)

used for each permeability measurement and the standard deviation average are calculated.

2.1. Concrete mixes

The following three concrete mixes (Table 1) with the same composition are studied:

- (1) Control concrete without swelling characteristics and cured for 28 days at 20 °C and relative humidity of 95 % (± 2 %) – this serves as a reference case
- (2) Concrete with coarse reactive siliceous limestone - susceptible to ASR
- (3) Concrete exposed to high temperature (80°C) during curing - susceptible to DEF

The composition is representative of a wide range of concrete used in French nuclear power plants, which must meet stringent durability requirements [40].

Cement consists of 92 % clinker, 6 % limestone, and 2 % secondary products such as slag and fly ash. The elemental composition of clinker is listed in Table 2.

To obtain significant expansion for the study, the alkali content must exceed the minimum threshold of 3 kg/m³ of equivalent alkali, as defined in [43,44] for instance. The natural alkali content of cement is 0.11 % for sodium oxide Na₂O and 1.36 % for potassium oxide K₂O, which gives a value of Na₂O_{eq} = 0.658 K₂O + Na₂O = 3.517 kg/m³. Therefore, the mixing water for both formulations was doped with NaOH to obtain 5 kg/m³ of Na₂O_{eq}, which is comparable to the material used in some previous works [13]. The NaOH pellets were added the day before each casting to prevent the increase in mixing water temperature during dissolution, which could affect the workability of concrete.

For both DEF and control concrete, non-reactive limestone aggregates are used. These aggregates have the following composition: 53 % CaO, 2.5 % SiO₂, 0.6 % Fe₂O₃, and 0.5 % Al₂O₃. The aggregates are angular in morphology, indicating they are crushed, and contain 0 % reactive silica. The real density of the aggregates is approximately 2637 kg/m³, with a water absorption capacity of 2.39 %.

Reactive aggregates are of a siliceous-limestone nature, 'Potentially Reactive' (PR). It is a highly studied aggregate in France, comparable to the Spratt aggregate from Canada, whose reaction products correspond well to those of ASR, with no trace of ACR observed. The real density of the aggregates is approximately 2657 kg/m³, with a water absorption capacity of 0.53 %. The full characterization is given in this article [45].

The following mixing sequence was adopted for the castings in this study:

1. Dry mix the components for one and a half minutes,
2. Add the NaOH-doped water with the entire quantity of superplasticizer, then mix for four minutes.
3. The specimens were cast in two layers, each vibrated for 15 seconds, to ensure proper placement and prevent segregation of concrete.

2.2. Protocols for conservation and conditioning of concrete expected to develop ISR

Various strategies for achieving optimal aging of concrete affected by ISR and for preconditioning samples for measuring air permeability of concrete can be found in the literature. In this study, the damaging strategies recommended by [46,47] have been adopted with some adaptations for the studied concrete mixes. This damaging procedure was chosen due to its representation of environmental conditions in damaged structures with similar concretes, as presented in [13] and [42]. Sections 2.2.1 and 2.2.2 explain the storage conditions for ASR and DEF to accelerate pathologies in the laboratory. The graphs show the thermo-hygrometric conditions after demoulding 24 hours after casting.

Table 2
Composition of clinkers.

Constituent	Elemental composition of clinkers (%)
SiO ₂	19.7
Al ₂ O ₃	4.6
Fe ₂ O ₃	3.2
TiO ₂	0.3
MnO	0.1
CaO	63.5
MgO	1.2
SO ₃	2.7
K ₂ O	1.36
Na ₂ O	0.11
P ₂ O ₆	0.5
Loss on ignition	3.6

2.2.1. Alkali-silica reaction

The development of ASR requires three essential elements: amorphous or non-crystalline silica from reactive aggregates, alkalis from the interstitial solution or external supply, and the presence of water. According to the previous study conducted by [3,48,49], a minimum relative humidity is necessary to generate expansion. The threshold humidity value depends on temperature conditions and the reactivity of the concrete.

The concrete ASR maturation protocol (similar to that proposed by [47]) is depicted in Fig. 4. After casting, specimens undergo autogenous curing by sealing them in plastic bags. They're stored at $20 \pm 2^\circ\text{C}$ and $95 \pm 2\%$ humidity for 28 days. Later, specimens are submerged in a $38 \pm 2^\circ\text{C}$ isothermal tank until testing. A centrifugal pump used to homogenize water inside a tank works by continuously circulating the water, ensuring uniform temperature and chemical composition in the tank solution. Thus, all the species leached from concrete during the specimen's conservation are not over-concentrated in the lower part of the tank (Fig. 1).

The immersion water is not replaced and is maintained at a volume 1.5 times that of the concrete. Additional water is added only to compensate for evaporation, which helps to prevent excessive alkali leaching during sample removal.

2.2.2. Delayed ettringite formation

The accelerated DEF protocol adopted for this study consists of three distinct steps presented in Fig. 2 [30,31]:

1. 30 minutes after casting, the specimens are stored in a climatic chamber to apply a thermal treatment for 7 days to create favourable conditions for the dissolution of primary ettringite at an early age, simulating a temperature rise at the core of a massive structure.
2. Specimens are demoulded at the end of the thermal treatment and the specimens are submitted to autogenous curing from 7 to 28 days.
3. Final immersion in water at 38°C to accelerate swelling kinetics.

During the autogenous curing, the specimens are wrapped in sealed plastic bags to prevent any water exchange with the outside and stored in the curing room at a temperature of $20 \pm 2^\circ\text{C}$ and a relative humidity of $95\% \pm 2\%$.

Prolonging the early heating period of concrete leads to an increase in the rate of expansion [50]. An optimum effect to maximize expansions has been demonstrated by calculating 'useful thermal energy' (UTE): it considers the heating duration after casting and temperature in a single parameter with a minimum threshold temperature of 65°C . It is the product of the heating duration and temperature. In Kchakech's study, the optimum is achieved for a UTE of around $1200^\circ\text{C}\cdot\text{h}$ with a maximum temperature of 81°C [50]. From a theoretical standpoint, the thermal treatment procedure adopted in the present study should generate a useful energy of $1179^\circ\text{C}\cdot\text{h}$, very close to the optimal value for maximum expansion development. With the intrinsic variations in the oven, a 5% error in the UTE could be acceptable.

Immediately after casting, the test specimens are placed in a climatic chamber to apply thermal treatment, up to 80°C for 3 days. The steps are explained by [1], and applied to concretes developing ISR.

The acceleration of DEF was achieved by maximizing the amount of ettringite destabilized at an early age; the thermal cycle used was controlled with a pre-setting period, a temperature elevation phase, with a heating rate of 2.5°C per hour, a period of maintaining a high temperature for 3 days, and finally, the cooling of the concrete with a cooling rate of 1.0°C per hour (Fig. 2 – [3,51]).

At the end of the curing period, the specimens, are submerged in an isothermal tank at a temperature of 38°C ($\pm 2^\circ\text{C}$), until test day with the ASR specimens.

2.3. Experimental program

The transport properties are measured at the following four states: (i) in the initial state after the curing period, i.e., without swelling (0%), (ii) with the onset of cracking (0.06%), (iii) with cracking of 0.12%, and (iv) significant expansion (0.22%). The method for expansions measurements is presented in Section 2.3.1. Regular measurement of expansion makes it possible to obtain the targeted levels. The specimens are then taken out of the storage tanks and dried to 80% saturation to stop expansions totally.

To characterize the air permeability, six saturation states have been chosen, four represent service conditions of structures. Wet

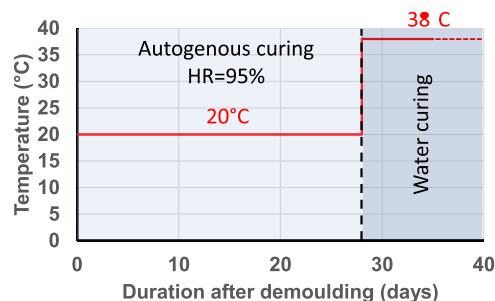


Fig. 1. Accelerated ASR conditioning test.

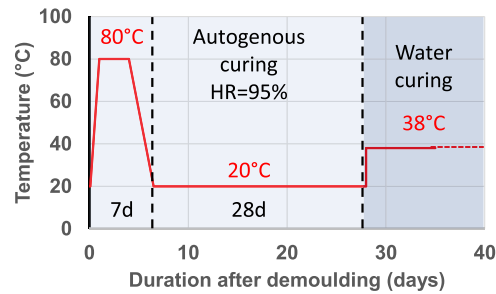


Fig. 2. Accelerated DEF conditioning test.

concrete (core or water-exposed areas, 80 % and 60 % saturation), dry concrete (regular sunlight exposure, 40 % and 20 % saturation). Two represent lab conditions, after drying at 80°C (about 3 % saturation), after drying at 105°C (standard saturation reference).

2.3.1. Expansion and mass monitoring

The advancement of ASR and DEF is commonly characterized by concrete expansion. The monitoring of expansions is based on the measurement of longitudinal deformation of the specimens using a needle extensometer. For this purpose, six studs forming three generators were glued in pairs along the height of the specimen. The pairs of studs were spaced at 100 mm (deformation measurement base) and were glued at an equal distance from the mid-height of the specimen. The generators are separated by 120° on the lateral surface of the specimen. Mass monitoring is performed by a scale that is accurate to the decigram. A schematic representation is shown in Fig. 3.

2.3.2. Microscopy

Scanning electron microscopy analyses were done on concrete samples with ASR and DEF. The central sample of the specimen was consistently used to minimize location-based variations in the sample. The samples were polished and carbon coated. The SEM used for the analysis is a JEOL 6380-LV model, equipped with a Bruker XFlash 6/30 EDS detector. The observations were conducted at an accelerating voltage of 15 kV, utilizing the Backscattered Electron (BSE) mode. Various magnifications were used, from x15 to x500, to estimate crack lengths and openings.

2.4. Protocols for transport properties

15 × 30 cm cylinders were cast. Tops and bottoms were cut off. Each cylinder was sliced into five pieces of 5 cm thick. Three were for transport measurement and air permeability testing, two for water porosity.

2.4.1. Water porosity

The water-accessible porosity test [52] and apparent density measurement are conducted following the hydrostatic weighing and complete drying. These tests quantify the volume of the connected porous network within the material that is in contact with the exterior.

In this study, the porosity is measured on samples with a diameter of 150 mm and thickness of 50 mm. They are placed in a desiccator under vacuum for 4 hours, then saturated in water for 48 hours in three successive steps. After saturation, they are weighed in water then wiped on the surface with a damp cloth and weighed in air. The porosity samples are then dried in an oven at 105°C until

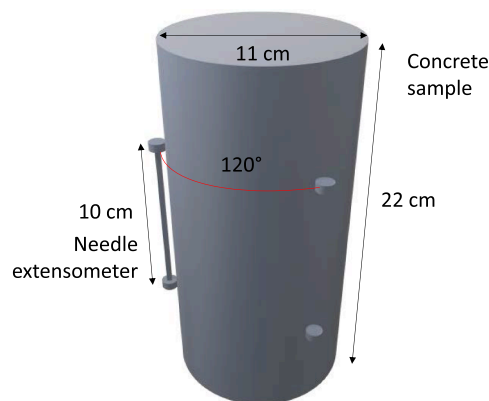


Fig. 3. Schematic representation of longitudinal extensometer measurements on three generatrices of concrete test specimens.

the mass stabilization, determined by a criterion of mass loss less than 0.05 % over one day. The porosity p , is measured after drying at 105°C. The purpose of drying at 105°C is to remove all free water; this temperature is recommended by the standard [53].

2.4.2. Mercury porosimetry

The tests follow the procedure in [54] and only one sample was tested for each concrete, for one expansion at a given saturation rate. A 1 cm³ sample is taken from the concrete sample, taking care not to over sample the aggregates to be representative of the cement paste. It is dried at 105°C until mass stabilization, and a vacuum chamber is used to remove the air contained in the pores. Incremental mercury pressure is applied to accurately reach pores between 1000 and 10 nm.

2.4.3. Drying kinetics

After autogenous curing or water immersion, concrete specimens were saturated and impermeable. Before measuring air permeability, draining some water from the porous structure is necessary. Drying duration is crucial for quantifying transport property, depending on the material's diffusivity coefficient. High-temperature drying can evaporate bound water in the sample's porous network, altering hydrates, ettringite, and ultimately C-S-H [55,56]. This study focuses on internal swelling reactions in concrete. Minimizing temperature effects on microstructure is crucial because ettringite is unstable around 65°C. Excessive speed can cause thermal gradients, leading to differential expansion cracks between the core and surface, and significant moisture gradients [57] throughout the sample thickness. Also, it can lead to cracking due to restrained shrinkage between aggregates and cement paste [3,58]. The proposed drying method involves stepwise increases in temperature, outlined in Table 3. Drying at 40°C continues until saturation levels reach around 30 %. Temperature then rises to 50°C to prevent prolonged drying at low saturation levels. Transitioning from 20 % to 3 % saturation, temperature is increased to 80°C, then to 105°C to reach 0 % saturation. Current knowledge suggests that drying microcracks are limited when temperatures do not exceed 50°C [57]. However, for temperatures higher than 80°C, it is established that additional damage occurs [59,60] along with dehydration of the products formed during internal swelling reactions. This approach could help to reduce moisture gradients and resulting shrinkage gradients, which were primarily the main cause of micro-cracking [38]. These micro-cracks can affect permeability measurements [61–64].

Specimens' lateral faces are covered with watertight aluminium to ensure one-way drying. Before permeability measurement and at the end of each drying cycle, concrete saturation is homogenized as specified by [61]. The specimens were sealed and placed in airtight bags in the oven at the same temperature for a duration at least equal to the last drying cycle. The complete homogenisation is difficult to obtain without homogenizing at least four times the drying time [38]. However, this step partially unifies the saturation within the sample, leading to homogeneous permeability values.

2.4.4. Air permeability

The measurement of air permeability on cylindrical specimens is performed using a constant-head permeameter of the Cembureau type according to the standard [65].

Specimens, 50 mm thick, are confined with an air chamber inflated to 8 bars to ensure lateral tightness. They undergo unidirectional airflow under a pressure gradient. Cembureau protocol has already been used for the air permeability measurement of concrete damaged by DEF [13,30], but the lateral confinement may result in partial reclosure of cracks, leading to an underestimation of air permeability in heavily cracked concretes. However, conducting permeability measurements on numerous specimens at various saturation rates without the Cembureau technique is challenging. Other methods for determining the permeability of cracked concrete are not easily scalable for numerous measurements [24]. Moreover, the literature reports that the reclosure of ISR-induced cracks requires significant compressive stress [66]. Thus, the reclosure of such cracks by a low radial confinement of less than 1 MPa is expected to be reduced, under the effect of compressive stress performed after expansion. To quantify the impact of lateral confinement, air permeability measurements on ISR-affected concretes have been performed with confinement pressures between 0.5 and 0.9 MPa [67]. In this study, the permeability reduction effect was always lower than 12 % for ASR-damaged concrete and 20 % for DEF-damaged concrete. These maximal reduction effects were obtained at the lowest saturations (3 and 0 %) on specimens with the largest expansion (0.22 %). It was lower for higher saturation and smaller expansion (between 3 and 7 % of flow reduction for saturation between 80 and 20 % and ASR expansion of 0.12 %). Therefore, the effect of confinement pressure was moderate because the faces of the cracks induced by ISR are not directly opposite each other, and the partial filling by swelling reaction products does not allow the reclosure of the induced cracks, by compressive tests. However, the permeability evaluated here should be considered as a low value of the increase of air permeability by ISR. The standard deviations are shown in the graphs as error bars. The value of apparent permeability ($k_{A0,2}$) is calculated from the average of three permeability samples for a relative injected pressure of 1 bar (0.1 MPa), corresponding to 2 bars (0.2 MPa) absolute pressure. Therefore, the apparent permeability is obtained according to the following equation [68,69]:

Table 3

Drying temperature to achieve the target saturation rates.

Saturation rate (%)	Maximum drying temperature (°C)
80, 60, 40	40
20	50
3	80
0	105

$$k_A = \frac{Q_o}{S} \frac{2\mu LP_o}{(P_i^2 - P_o^2)} \tag{1}$$

Where: k_A : the apparent permeability obtained (m^2), Q_o : the volumetric flow rate (m^3/s), μ : the dynamic viscosity of air (Pa.s), L : the thickness of the sample (m), P_o : the absolute pressure at the outlet (Pa), S : the cross-sectional area of the sample (m^2), P_i : the absolute pressure at the inlet (Pa).

3. Results

3.1. Expansion and cracking

Fig. 4 presents the mass variation for the three types of concrete, control, ASR, and DEF, during immersion at 38°C. In grey the control concrete, in blue DEF and in orange ASR.

DEF concrete shows a significant increase in mass, reaching around 1.6 %, reflecting significant moisture absorption or water retention due to the formation of by-products such as delayed ettringite. In comparison, ASR concrete shows a more moderate increase with a plateau around 0.6 % after about 100 days, probably due to water absorption associated with the formation of expansive gels typical of the alkali-silica reaction. The control concrete, on the other hand, remains stable with a low variation in mass of about 0.4 %, indicating minimal water absorption typical of a material not affected by pathological reactions.

Fig. 5 presents the deformation for the three types of concrete, control, ASR, and DEF, during immersion at 38°C. In grey the control concrete, in blue DEF and in orange ASR.

The control concrete exhibits only a slight expansion due to water absorption during immersion. The maximum expansion of this concrete reaches 0.02 % and does not exceed the expansion limit threshold set by standards. This limit qualifies concrete as susceptible to ISR under accelerated conditions (0.04 %). This expansion is typical for concrete immersed in water and is due to the decrease in capillary tensions originally generated by autogenous shrinkage. The expansion curve for ASR exhibits a usual sigmoidal shape and can be characterized into three stages [10,48,49,70]: latency period, expansion acceleration and stabilization period. The Larive’s model is used to fit the two ISR expansion. The following equation is given for ASR:

$$\epsilon_{ASR,exp} = \epsilon_{\infty} \frac{1 - e^{-\frac{t}{\tau_k}}}{1 + e^{-\frac{t - \tau_{lat}}{\tau_k}}} \tag{2}$$

The calibration parameters used for ASR are: ϵ_{∞} =0.280 %, τ_{lat} = 81.48d and τ_k = 23.62d. With ϵ_{∞} : the asymptotic expansion, τ_{lat} : the latency time and τ_k : the characteristic time.

Transitions from the latency period to the acceleration phase occur at about 35 days (Fig. 5). The acceleration phase lasts approximately 100 days before entering the stabilization period indicating that probably some of the factors involved in the ASR had become exhausted [71]. The final expansion does not exceed 0.28 %. The progressive increase in the standard deviations of ASR expansions, especially beyond 0.20 % expansion, indicates a growing localization of open cracks in the specimens. These results are in accordance with the four cracking propagation stages described in [72]. Cracks form within the aggregate particles in the early stages of the reaction, then extend into the cement paste with increasing expansion to eventually connect the reactive aggregate particles in an extensive cracking network. This crack evolution lead to the increase of expansion variability.

DEF exhibits three phases similar to ASR, with a sigmoidal shape [73,74]. The calibration parameters used for DEF are: ϵ_{∞} =0.355 %, τ_{lat} =204.87d and τ_k =70.66d. The latency phase lasts about 65 days. The acceleration phase is less steep and longer than ASR’s. DEF’s stabilization phase is a deceleration rather than a pronounced stabilization. DEF’s final expansion level reaches nearly 0.35 %, with no slowdown in kinetics [73].

ASR and DEF reached 0.22 % expansion at 110 and 250 days respectively. Transport properties were measured on control specimens at these ages to assess hydration effects. Standard deviations of expansions for DEF and control concrete were negligible (<0.004 %), indicating minimal cracking.

For the expansion of 0.22 %, the localized cracks with an opening larger than 100 μm are observed for ASR (Fig. 6), and dense cracking with a small opening (usually lower than 40 μm) for DEF (Fig. 7).

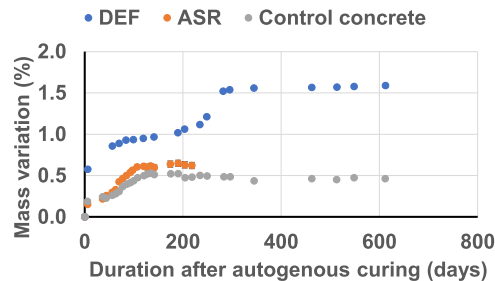


Fig. 4. Mass variation for the control concrete, ASR and DEF.

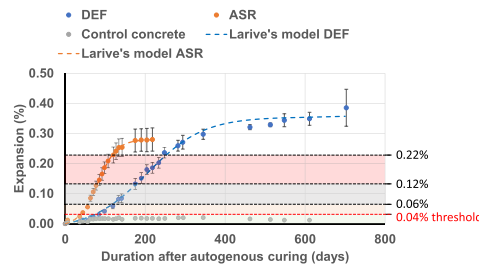


Fig. 5. Expansion kinetics for the control concrete, ASR and DEF.

ASR cracking can be divided into two categories. The first one is due to the alkali concentration gradient between the core and surface of the specimens for conservation in moisture or water [29]. This gradient results in the localized cracking that is visible to the naked eye, very open but shallow [75,76]. The second is cracking in the aggregate, which gradually spreads into the cement paste, and could fracture the aggregate [72]. The disparate morphologies of the two types of cracks are anticipated to yield differing effects. The initial category arises from edge effects and is contingent upon the geometric attributes of the damaged elements. Consequently, it inadequately characterizes the material’s permeability and may induce scale effects contingent upon the dimensions of the damaged constituents, necessitating its consideration in result analysis. Conversely, in the case of DEF, the crack network manifests greater density, attributed to product formation within the concrete porosity. Typically, localized cracks are not observed, obviating the need for distinguishing crack types in the analysis of permeability results.

3.2. Transport properties

3.2.1. Water porosity

Fig. 8 shows water porosity evolution based on expansion from internal swelling reactions. Control concrete is shown in grey, DEF in blue, and ASR in orange.

The water porosity of the control concrete is around 16 % and remains relatively stable over time, increasing slightly from 16.2 % initially to 16.5 % after 249 days in water, which remains within the usual variability of this test. During water immersion, the porous network experiences no notable volumetric changes due to cement hydration. Similar behaviour can be anticipated for ASR-damaged concrete under similar curing conditions. Therefore, the evolution of water porosity in concrete damaged by ASR cannot be detected by this common test.

The initial difference in water porosity between ASR concrete (less than 15 %) and control concrete arises from variations in aggregate composition and distribution. The mineralogical makeup of aggregates influences the interfacial transition zone at the paste/aggregate interface, impacting concrete’s porosity and mechanical properties [73,74,77]. Furthermore, the presence of fines in castings with siliceous aggregates might partially account for this distinction. After autogenous curing, the water porosity of the concrete used to create DEF is approximately 17 %. The initial porosity difference with the control concrete primarily results from early curing of DEF. The heat treatment up to 80°C for DEF specimens yields two effects that contribute to the rise in water porosity: accelerating hydration and forming various hydrates, as well as potentially inducing delamination at paste-aggregate interfaces due to differential thermal expansion [57,78,79].

The difference in crack localization between ASR and DEF is seen in the coefficient of variation of porosity analysis. ASR has higher variation due to few open cracks, while DEF shows more uniform small cracks. ASR skin cracks cause an increase in apparent volume, not detectable during hydrostatic weighing, as the cracks may drain between water and air weighing. This seems to occur for ASR-damaged concrete. During DEF expansion, damaged concrete’s porosity increased from 17 % to 18.3 % with a 0.22 % expansion,

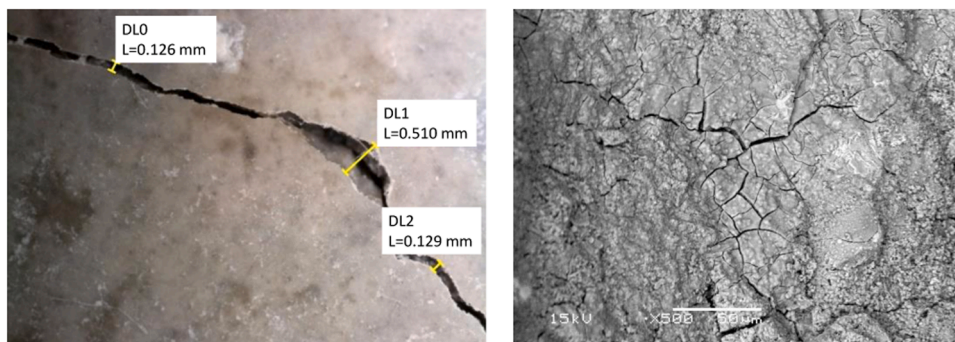


Fig. 6. Cracking pattern for ASR and products in the crack (SEM) for expansion of 0.22 %.

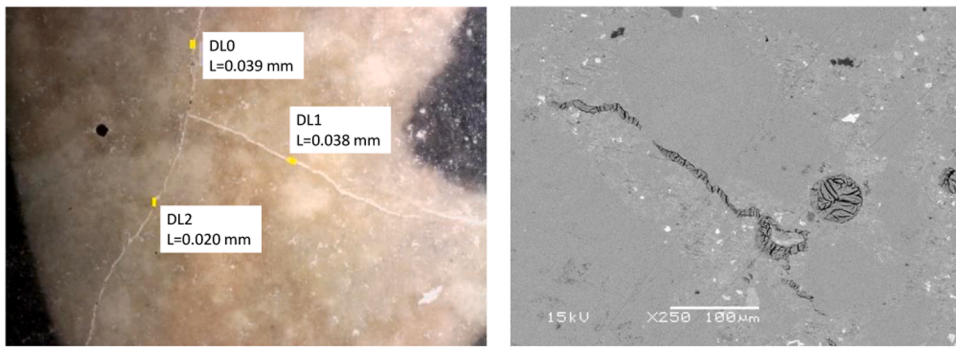


Fig. 7. Cracking pattern for DEF and products in the crack (SEM) for expansion of 0.22 %.

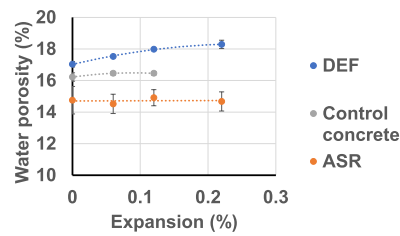


Fig. 8. Water porosity of concrete damaged by ASR and DEF.

consistent with previous findings [13].

3.2.2. Mercury porosimetry

The mercury porosimetry curves for the three types of concrete are shown in Fig. 9. (a) represents the mercury porosimetry for control concrete, (b) for ASR and (c) for DEF. The tests for each type of concrete and each level of expansion were conducted on a single sample. For the control concrete, the curves are based on age after the end of the autogenous curing. For concrete affected by ISR, porosimetry has been evaluated for the initial stage and the three targeted expansions.

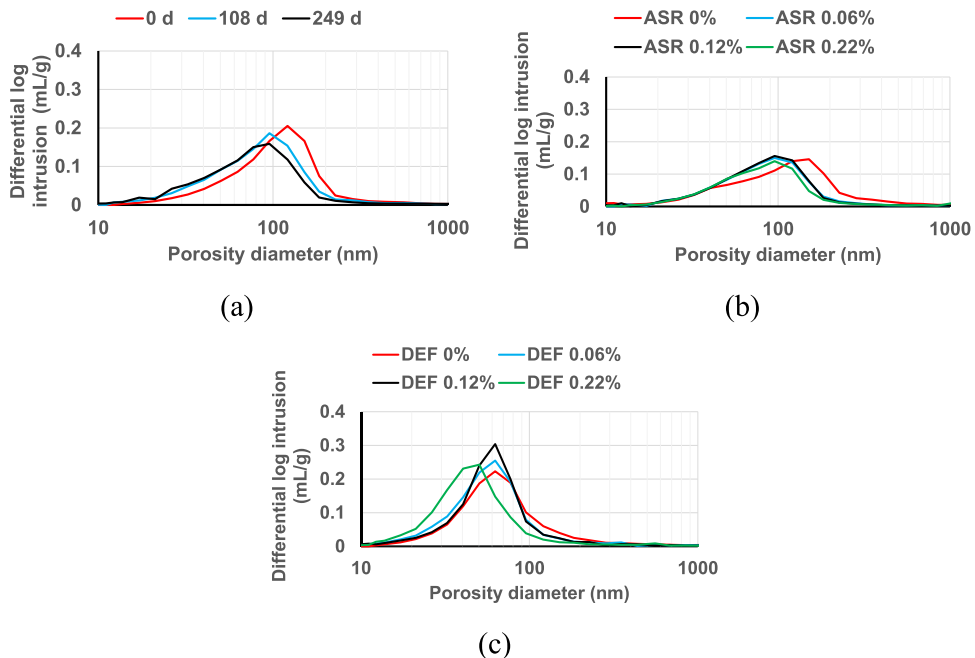


Fig. 9. Mercury porosimetry curves as a function of duration after curing for the (a) control concrete, (b) or expansion for ASR, (c) and DEF.

The analysis of the mercury porosimetry presented in Fig. 9 is performed through the analysis of the average pore radius and the total intrusion volume thereafter.

Fig. 10 presents the total intrusion volume and Fig. 11 the average pore radius of pores smaller than 10 μm, deduced from the mercury porosimetry, for the control concrete (according to age after curing period) and for concrete damaged ASR and DEF, respectively.

The three concretes in their initial state, without pathological development, have a similar mercury intrusion volume of about 0.11 mL/g. DEF concrete shows an increase of 8 % at 0.06 % strain, stabilizing at about 5 % at 0.12 % and 0.22 % strain. ASR concrete shows a decrease of about 10 % at 0.06 % and 0.12 % strain, followed by a 15 % decrease at 0.22 % strain. The control concrete shows a 5 % reduction after 249 days of curing. These results are consistent with the water porosity results presented in Section 3.2.1. The DEF concrete undergoes diffuse damage within the cement paste, coinciding with the delayed formation of ettringite. This increase in porosity leads to expansion of the pore network and cracking.

In contrast, the competition between damage and ASR gel formation does not result in significant change at the volumetric level. In the control concrete, the incomplete curing process refines the pore network and densifies the cementitious matrix.

In addition, regarding the influence of alkali addition on hydration, it is well documented that alkalis can accelerate the hydration of certain cement phases, particularly C3A and C3S, by raising the pH and promoting the dissolution of clinker phases [80]. This acceleration typically results in the rapid formation of hydration products such as calcium silicate hydrates and ettringite, leading to a denser microstructure in the early stages of hydration [16,81].

However, at later stages, the continued presence of alkalis can alter the pore structure through secondary reactions. For example, in ASR-prone environments, alkalis promote the formation of alkali-silica gel, particularly in the presence of reactive aggregates. This gel can partially fill pores, thereby locally reducing porosity, but it also induces swelling pressures that lead to microcracking in the cementitious matrix. These competing effects significantly influence the pore size distribution by creating a more heterogeneous network of pores and microcracks.

The difference in mean radius between control and ASR concrete is less than 12 % because the effect of ITZ is not detectable with the mercury porosity instruments used here. The difference in mean radius between control and DEF concrete is significant due to the thermal curing at an early age. The differences in the hydration reactions according to curing conditions can lead to the refinement of the pore network and the formation of different hydrates, with lower C/S ratio, resulting in the formation of denser C-S-H [10,82].

Mercury intrusion volume does not change over time for control concrete, meaning that there is no volumetric change in the 10 to 1000 nm porosity range. However, there was a decrease in the average pore radius between 0 and 109 days, reflecting continued hydration facilitated by storage in water at 38°C [83].

For ASR, the volume of mercury intrusion decreases slightly, and the mean radius also decreases with the development of pathology with time. The same conclusions can be drawn for the control concrete with the effect of cement hydration on the mean radius. Since the measurement technique does not detect ITZ or cracks caused by internal swelling, both of these are generally greater than 1 μm, microstructural changes are not apparent at this scale of measurement, except for the continued hydration.

For DEF, there is also no change in the volume of mercury intrusion. There is a slight decrease in pore radius at 0.22 % expansion, but no significant change, as the hydration is more advanced than for the two previous concretes due to thermal treatment at an early age.

Overall, mercury porosity provides information on microstructural evolution for pore radii between 10 and 1000 nm. This highlights hydration trends over time for concretes stored in water at 38°C. However, cracking due to swelling, with crack openings generally larger than 20 μm, and ITZ between paste and aggregate are not detectable by this measurement.

3.2.3. Drying kinetic

Fig. 12 presents the drying times required to achieve the target saturation levels for the three types of concretes with aging and

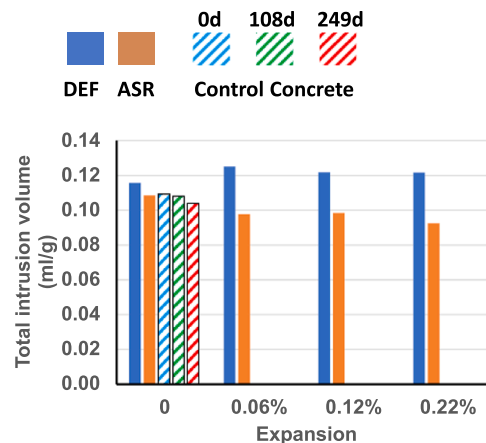


Fig. 10. Total intrusion volume for control concrete and concrete damaged by ASR and DEF.

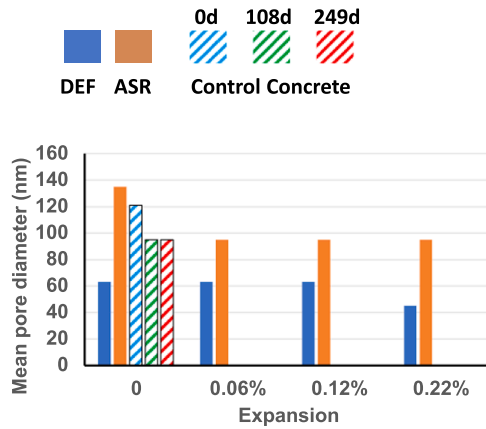


Fig. 11. Mean pore diameter for control concrete and concrete damaged by ASR and DEF.

expansion. The heating temperatures were 40°C until reaching 40 % of saturation, then were set to 50°C.

A comparable drying rate is noted in the control concrete from 80 % to 40 % saturation, regardless of the material’s age but there appears to be a very slight tendency toward faster drying for the 0.22 % expansion. It appears that the advancement of hydration does not exert a significant influence within this moisture range. Below 40 % saturation, a prolonged drying time is necessary, potentially attributed to the observed decrease in the mean radius of porosity and consequently greater hydration after 249 days of water curing.

Regarding concrete damaged by ASR, no trend is observable, the difference is of the same order as that of the scatter. Despite ASR-induced expansion and cracking, the drying kinetics exhibit uniformity both with and without expansion for this type of drying up to 20 % saturation and at corresponding temperatures of 40 and 50 °C, consistent with findings reported in [84].

When comparing the different drying times for the various types of concrete, it is observed that the drying time for the concrete damaged by ASR is higher than the other two, which corroborates with the results observed in water porosity, with the smallest porosity for the concrete used to obtain ASR. It seems that the overall water porosity is the best predictor of drying kinetics, up to 20 % for the concretes studied here.

The effect of a very diffuse and dense cracking caused by DEF on drying time could be more important than the effect of localised cracks due to ASR.

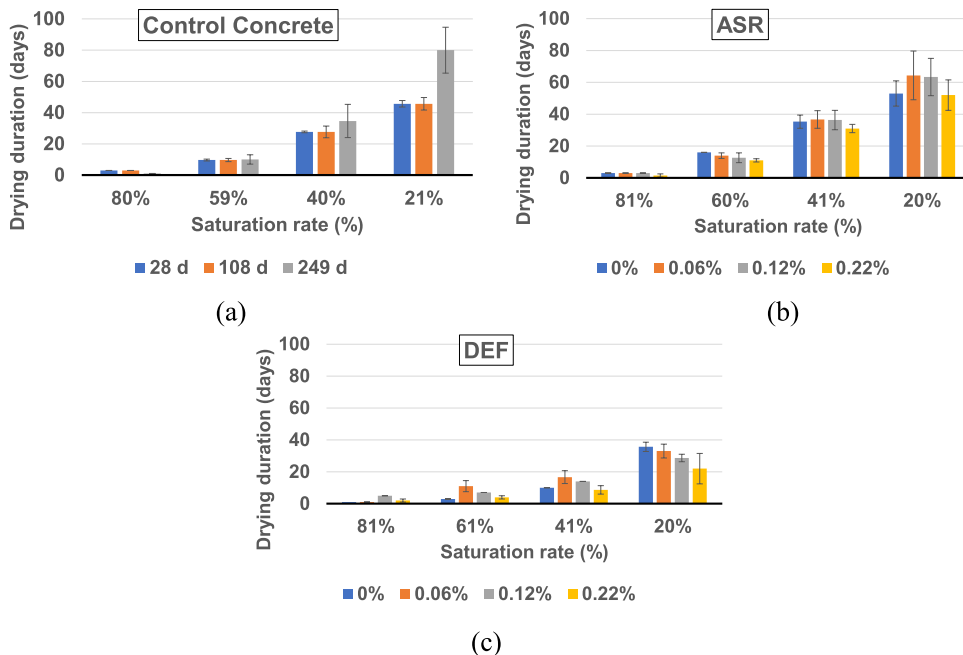


Fig. 12. Drying duration for (a) control concrete, (b) concrete damaged by ASR (b) and (c) concrete damaged by DEF.

3.2.4. Apparent permeability at 2 bars

This section analyses apparent permeability at 2 bars of absolute pressure for each concrete relative to saturation and expansion or age for the control concrete. Fig. 13 illustrates apparent permeability for the three concretes. Special focus is given to (a) control concrete, (c) ASR, and (e) DEF, examining permeability for saturations between 80 and 20 % to highlight ISR's effect on permeability in service conditions. (b), (d), and (f) depict results for measurements conducted under standard conditions (after drying at 80 and 105°C).

For the control concrete, permeability remains consistent across the three measurement periods throughout the saturation range. Evolution curves show similar trends and magnitudes. Generally, the concrete is airtight up to 60 % saturation. Beyond that, permeability increases almost linearly between 60 % and 20 % saturation. At lower saturations, there is a noticeable trend towards a sharp rise in permeability. These results align with what's typically observed in the literature [85].

The ASR induced concrete has a permeability 3.7 times greater than the control concrete prior to expansion. Both have undergone

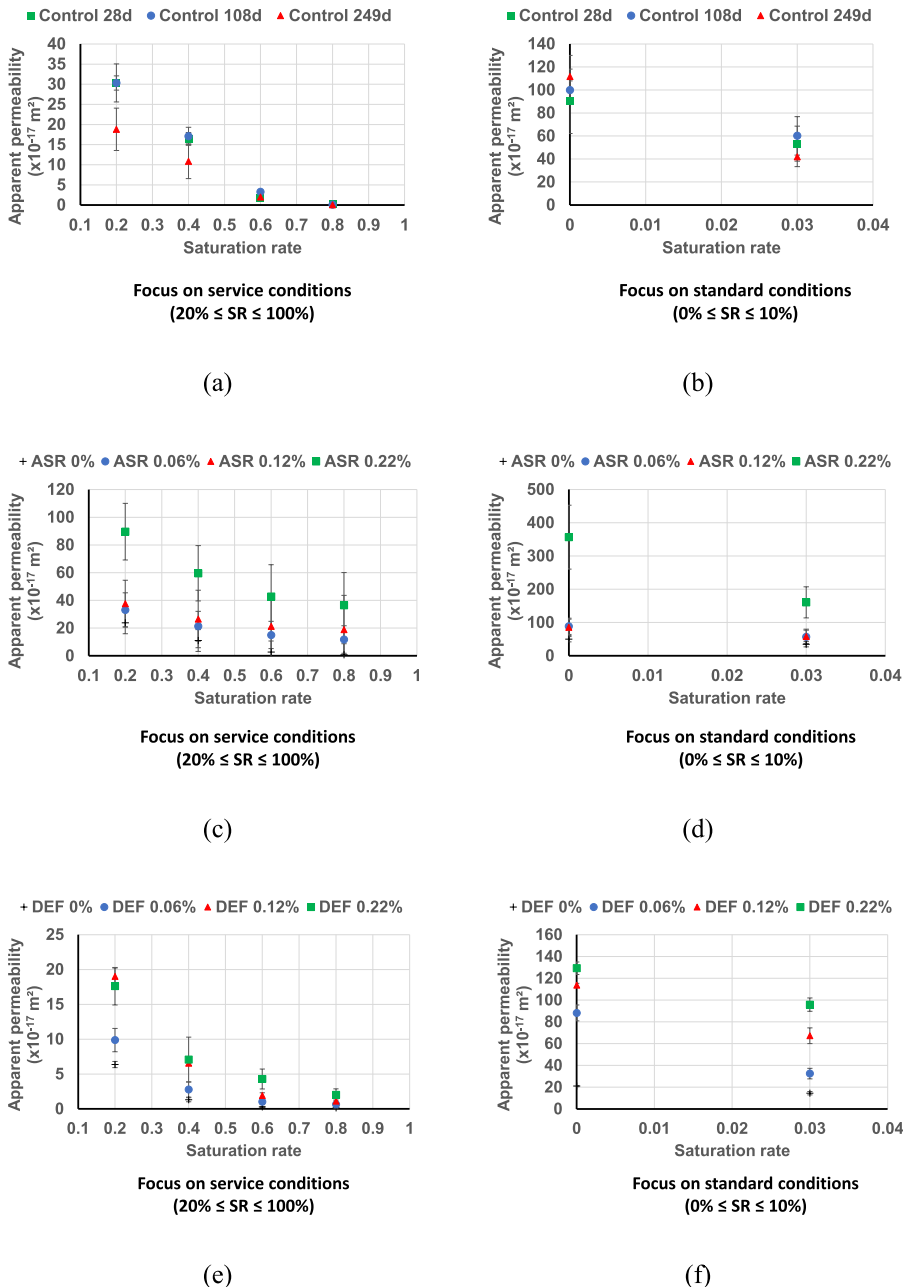


Fig. 13. Apparent permeability for control, ASR and DEF concretes in service conditions (respectively a, c, e) and for standard conditions (b, d, f).

the same curing conditions, the difference being water porosity and pore size. The latter parameter seems to be predominant. Conversely, the DEF concrete is about 1.6 times less permeable than the control, probably due to early hydration effects obtained during thermal activation. The thermal cycle in this study increased porosity and water diffusivity, which is consistent with the findings on chloride ion diffusivity in previous studies [13,86]. Early thermal curing also resulted in finer pore radii in the network, leading to a decrease in air permeability.

Air permeability of concrete damaged by ISR is significantly impacted both for ASR and DEF, particularly for high saturation degrees. The effects seem to be different for the two ISRs. The evolution of permeability with ISR based on Fig. 13 is analysed in the following discussion.

Variability in permeability observed here for ASR and DEF is correlated with expansion. It has been shown that for significant expansions in ASR, the variability progressively increases. This is due to the presence of widely open cracks. In DEF, the much more homogeneous cracking at the material scale leads to lower variability in permeability values.

4. Discussion

4.1. Evolution of air permeability with ASR and DEF

The permeability values given here are the low values of air permeability. As explained in Section 2.4.4, the closure of certain cracks alters the permeability.

The difference between the permeability of damaged concrete, k_{exp} , and the initial permeability, k_0 , has been plotted according to the saturation for expansions of 0.06 % in blue, 0.12 % in red, and 0.22 % in green (Fig. 14). The y axis represents the difference of permeability $k_{exp} - k_0$. It is the part of the air permeability due to the cracks induced by ISR, without the effect of the initial pore network. The x axis are the saturation rates studied.

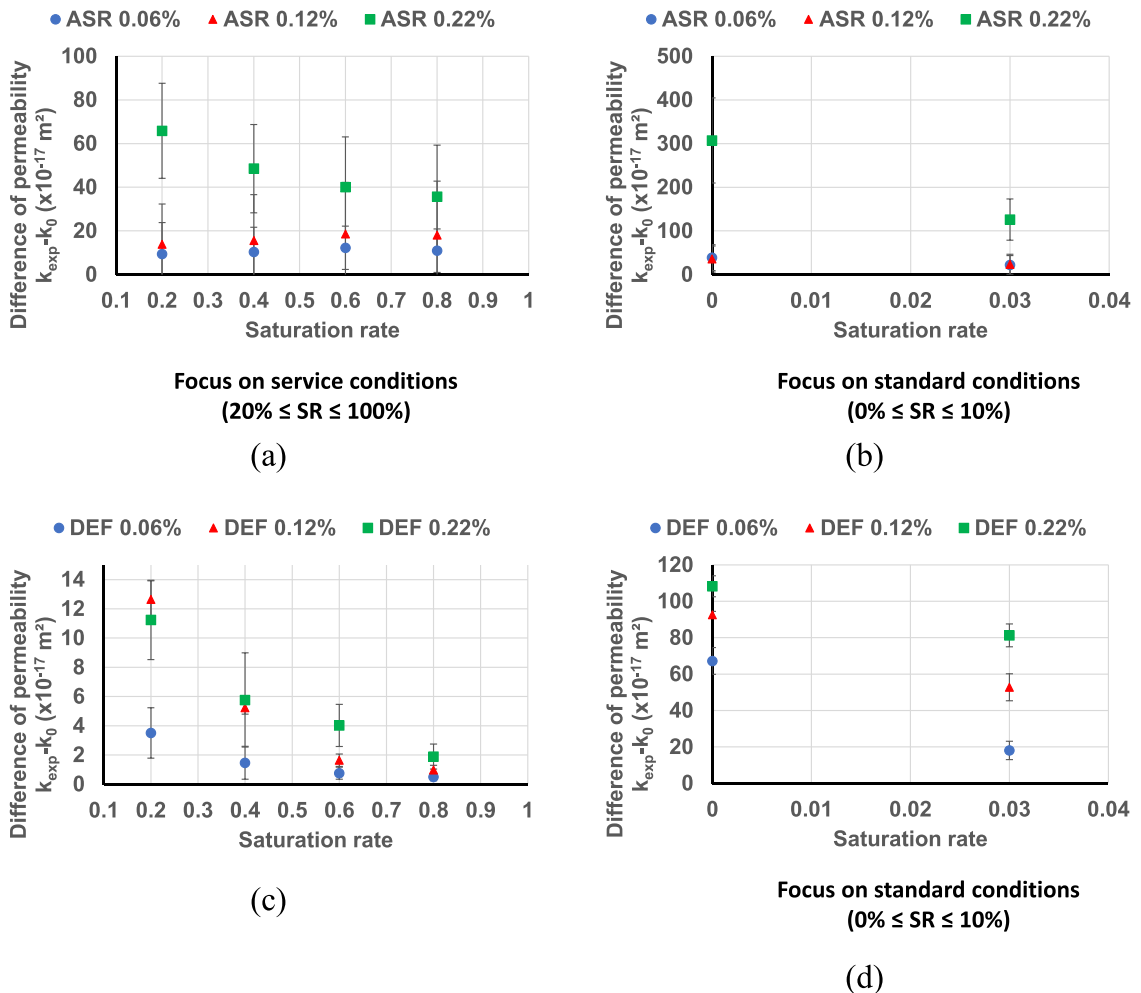


Fig. 14. Difference of permeability, $k_{exp} - k_0$, for ASR and DEF in service conditions (a, c) and for standard conditions (b, d).

The evolution of permeability with ASR at 0.06 % and 0.12 % shows plateau in service conditions. The cracking contribution to permeability is present from 80 % saturation and remains stable until 20 %. At 3 % and 0 % saturation, the crack contribution increases by a factor of 2. It is important to note the absence of dependence on saturation of the contribution of ASR-induced cracks for these small expansions at high saturations (service conditions).

Under the microscope, the observed cracks have an average opening of 150 micrometers. According to the Hagen-Poiseuille equation [87], this increase in permeability is consistent with a crack length of 50 mm, the thickness of the sample. The observed crack opening of 150 micrometers matches the physical observations. From 80 %, cracks with such openings are removal of water. This can explain why it is not dependent on saturation. It also highlights that the transport through the pore network does not show evolution at these levels of expansion for high saturations. It can be explained by localisation of ASR cracks mainly in the aggregate with little connection in the cement paste, similar to that observed in [71,72]. The evolution observed for low saturations (3 and 0 % for standards) can be explained by a combination of cracks induced by drying during the conditioning process. In specimens already damaged by ASR, drying cracks can be initiated and have an easier propagation than in the concretes without ASR. It leads to the combination between the different cracks and to this important increase which is not representative of what happens in structures.

For ASR at 0.22 %, a slight increase in the permeability of concrete can be noted from 80 % to 20 % saturation. The permeability of concrete at 3 % and 0 % is multiplied by a factor of 2, then 6 compared to 20 %. Cracks initiated in aggregates propagate to cement paste [72], contributing to the increase of the permeability by localized cracks and by a larger connection in concrete due to multiple cracks in aggregates connected with the initial pore network.

In DEF, permeability evolution with induced cracking shows significant divergence: contribution steadily rises as saturation decreases. Interestingly, crack contribution stays relatively low at 80 % saturation, unlike ASR. Under service conditions, fine DEF-induced cracks enhance pore network connection without localized cracks. At low saturations, particularly 3 % and 0 %, permeability significantly increases, suggesting strong connectivity and dense pathology-induced cracking. This indicates that higher expansion leads to greater connectivity, as induced cracking diffuses within the material.

Fig. 15 (a) and (b) present the relative permeability $k_{exp}(Sr)/k_0(Sr)$ for concretes at various saturation levels and exposed to ASR and DEF, respectively. This represents the quotient for each expansion between the permeability measured at this expansion rate for a given saturation and the permeability measured at the initial state for the same saturation. The error bars on a logarithmic scale can appear very large or very small according to the localisation of the dots along the vertical axis. This is due to the nature of the scale. This scale compresses or expands the distances between values non-linearly.

The relative permeability exhibits minimal evolution at 20 % of saturation for both concretes, regardless of the expansion level. This indicates minimal impact of cracking induced by ISR at 20 % of saturation. The most pronounced effect for ASR is at high saturation levels (the permeability is multiplied by 40 at 80 %). Pathological cracking significantly contributes to percolation starting from 80 %, a new finding in the literature. Under 20 % saturation, pathological cracking plays a predominant role at lower saturation levels of 3 % and 0 %, albeit to a lesser extent. For DEF concrete, similar to ASR, there is a strong contribution at 80 % and 60 % saturation from pathological cracking, forming a plateau. Then, the relative contribution decreases, as for ASR, the part due to the initial pore-network taking precedence over the permeability induced by DEF.

For lower saturation degrees (3 and 0 %), the increase of relative permeability compared to 20 % saturation can be explained by a greater appearance of cracks due to drying at high temperatures (80 and 105 °C) in concrete damaged by ISR than in concrete before ISR. The dehydration of products formed by ISR by these high temperatures leads to a certain release of the pore network involved in permeability transport, which probably also contributes to this increase.

High saturation causes increased permeability, especially at 80 %, due to significant crack opening. Concrete is typically impermeable at these levels. Limited interaction occurs between existing porous networks and ASR cracks. DEF's dense, diffuse cracking ensures strong interaction with the porous network.

4.2. Evolution of transport properties with ISR-induced cracking

For ASR, there is no change in water porosity. This can be attributed to disruption of hydrostatic weighing or insufficient modification of the overall volume to be detectable. No changes in mercury porosimetry have been observed according to the detection range of the equipment, which does not allow for highlighting modifications at the interface transition zone (ITZ) or in the cracks with an opening larger than 10 μm . The drying time and diffusivity are not affected by ASR-induced cracking, regardless of the expansion level between 0.06 % and 0.22 %. However, the open and localized cracking strongly impacts permeability, especially at high saturations from 80 % onwards. This is particularly true when expansion is significant high.

For DEF, expansion within concrete leads to a significant increase in water porosity. The modifications in mercury porosimetry did not show any conclusive evidence regarding the progression of the pathology. There seems to be a tendency to increase the drying rate with increasing expansion, especially at 20 % saturation. Permeability could be multiplied by 44 compare to the initial value, especially at high saturation levels for ASR and 1.8 for DEF. These results can be correlated with the type of cracking induced by each pathology and by their progressive filling by the products formed during the aging. ASR produces two types of cracking: the first one is a macroscopic cracking at the surface of the specimens due to the alkali gradient. It is a localized cracking at the sample scale. The second type of cracking begins from the core of aggregates. Then, propagates through the aggregates, ITZ and cement paste. This makes the granular part permeable and highly connected to the concrete pore network. Cracks due to ASR are usually partly filled by hydration products but the rate of filling of cracks is low [72]. On the other hand, DEF involves microscopic diffuse cracking with high density and interaction with the existing porous network. DEF-induced cracks are often observed as largely filled by ettringite (Fig. 7). ASR-induced cracks do not lead to an increase in drying kinetics. Their total specific surface is not sufficient to modify the drying rates,

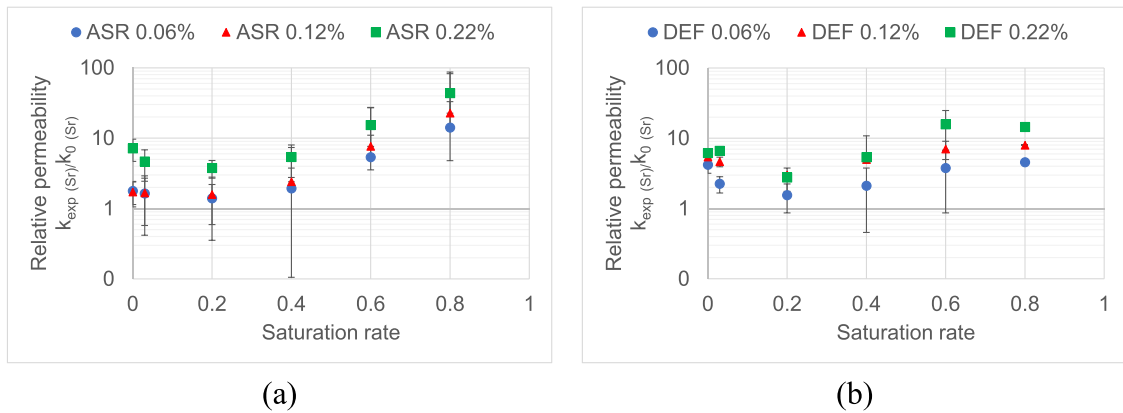


Fig. 15. Relative permeability, $k_{\text{exp}}(Sr)/k_0(Sr)$, for ASR(a) and for DEF (b).

unlike DEF-induced cracks. DEF-induced cracks provide a significant increase in specific surface area, conducive to an acceleration of drying. However, the significant opening of ASR-induced cracks, plays a predominant role in increasing permeability, especially since the granular part of the material is no longer impermeable at 0.22 % for high saturation rates. For DEF, the extremely high density of cracks, with openings ten times smaller, offers a much larger potential drying surface area. Therefore, drying is accelerated with increasing expansion for low saturations, due to the probability of interconnection with drying-induced cracking.

4.3. Importance for modelling

This study is pertinent for modeling, particularly in numerical analyses seeking to elucidate the coupling between the chemical advancement and the evolution of mass transport during crack propagation due to ISR. The influence of ISR on water diffusivity under drying conditions is marginal, with no discernible impact observed for ASR and only a slight augmentation noted for DEF. However, permeability is strongly affected by both pathologies, which is crucial for calculating leakage flow rates in containment structures. The high dependence of permeability on expansion level is also an important concern for dams damaged by ISR. The data presented in this paper can be used to evaluate the evolution of concrete permeability due to ISR-induced cracks without perturbation related to reaction mechanisms between the fluid and the concrete. This is a key parameter to model this highly combined thermo-hydro-chemo-mechanical problem with minimal interaction between the different mechanisms.

The present work is the first tentative to quantify the effect of ISR on permeability in parallel to the three other transport properties with the standardized method. Next, it will be completed by a test performed with a new measurement device currently under development in the laboratory that eliminates the effect of confining pressure. In conclusion, improving methods for monitoring permeability and saturation in massive structures is critical to ensuring their performance and durability. The proposed approaches, such as advanced instrumentation and numerical modelling allow a better understanding and anticipating for variations in these properties and thus more effectively manage the associated risks.

5. Conclusion

The characterization of mass transport properties in structural concrete is essential to evaluate leakage evolution in containment structures damaged by ASR or DEF. These chemical attacks induce swelling and internal cracking with different patterns, requiring transport property quantification under realistic saturation conditions for operating structures.

The main conclusions of this work are as follow:

- ASR does not significantly alter porosity or diffusivity but has a marked impact on air permeability due to localized cracking. For an expansion level of approximately 0.06 %, ASR increases permeability by more than 10 times compared to undamaged concrete, even under high saturation conditions, meaning that cracks occur at early expansion level.
- DEF slightly accelerates drying with increasing expansion and significantly modifies permeability. It produces finer and denser cracks compared to ASR at similar expansion levels. For an expansion level of approximately 0.06 %, DEF increases permeability by about 4 times compared to undamaged concrete.

The permeability evolution of concretes damaged by ASR and DEF reflects the differences in crack pattern produced by these two degradation mechanisms:

- ASR produces macroscopic skin cracks. These surface cracks have a significant effect on air permeability, and this effect remains independent of saturation conditions for expansions less than or equal to 0.12 %. Above this threshold, the progression of microstructural cracks extending from the interior of the aggregates towards the cement paste leads to an increased connection

between the initial porous network and this newly formed network of cracks. This leads to a significant increase in permeability throughout the volume of the damaged concrete.

- (b) DEF on air permeability is strongly dependent on the degree of saturation. This dependence results in the absence of macroscopic cracking for DEF expansions up to 0.22 %. The cracking that does occur is mainly microcracking, diffuse and closely associated with the initial pore network.

Practical implications:

- (a) The consequences of ISR-induced permeability changes on leakage are significant and must be considered in the management and maintenance of containment structures.
- (b) Empirical laws can be developed from this study to describe the evolution of permeability with expansion and damage, enabling assessments of ISR effects on leakage in structural concrete.

CRedit authorship contribution statement

Hugo Cagnon: Writing – review & editing, Writing – original draft, Visualization, Validation, Supervision, Methodology, Investigation, Formal analysis, Data curation. **Joe Maalouf:** Writing – review & editing, Writing – original draft, Investigation, Formal analysis, Data curation. **David Bouhjiti:** Writing – review & editing, Resources, Project administration, Funding acquisition. **Jérôme Verdier:** Writing – review & editing, Writing – original draft, Visualization, Validation, Supervision, Software, Methodology, Investigation, Formal analysis, Data curation, Conceptualization. **Jacques Jabbour:** Validation, Project administration, Funding acquisition. **Stéphane Multon:** Writing – review & editing, Writing – original draft, Visualization, Validation, Supervision, Software, Resources, Project administration, Methodology, Investigation, Funding acquisition, Formal analysis, Data curation, Conceptualization.

Declaration of Competing Interest

The authors of this article, Joe Maalouf, Hugo Cagnon, Jérôme Verdier, Jacques Jabbour, Stéphane Multon, David Bouhjiti, declare that they have no conflicts of interest to disclose regarding this research.

We wish to confirm that we have no financial, personal, or professional relationships with any individuals or organizations that could potentially influence our work inappropriately. Additionally, no sources of funding were received for this research that could create a conflict of interest.

Acknowledgements

This work was conducted as part of a collaboration between the Laboratory of Materials and Durability of Constructions from Toulouse and the Institute of Radioprotection and Nuclear Safety in France within the Consortium CONCRETE.

Data availability

Data will be made available on request.

References

- [1] E. Grimal, A. Sellier, S. Multon, Y. Le Pape, E. Bourdarot, Concrete modelling for expertise of structures affected by alkali aggregate reaction, *Cem. Concr. Res.* 40 (4) (2010) 502–507, <https://doi.org/10.1016/j.cemconres.2009.09.007>.
- [2] G. Giaccio, R. Zerbino, J.M. Ponce, O.R. Batic, Mechanical behavior of concretes damaged by alkali-silica reaction, *Cem. Concr. Res.* 38 (7) (2008) 993–1004, <https://doi.org/10.1016/j.cemconres.2008.02.009>.
- [3] H.F.W. Taylor, C. Famy, K.L. Scrivener, Delayed ettringite formation\$, *Cem. Concr. Res.* (2001) 11.
- [4] M. Collepardi, A state-of-the-art review on delayed ettringite attack on concrete, *Cem. Concr. Compos.* 25 (4-5) (2003) 401–407, [https://doi.org/10.1016/S0958-9465\(02\)00080-X](https://doi.org/10.1016/S0958-9465(02)00080-X).
- [5] T.C. Powers, Structure and physical properties of hardened portland cement paste, *J. Am. Ceram. Soc.* 41 (1) (1958) 1–6, <https://doi.org/10.1111/j.1151-2916.1958.tb13494.x>.
- [6] S. Jacobsen, J. Marchand, B. Gerard, Concrete cracks I: durability and self healing - a review, in: J. Marchand, B. Gerard, S. Jacobsen (Eds.), *Advances in Concrete Durability*, CRC Press, Boca Raton, 2004, pp. 1025–1035.
- [7] Y. Fu, J.J. Beaudoin, Microcracking as a precursor to delayed ettringite formation in cement systems, *Cem. Concr. Res.* 26 (10) (1996) 1493–1498, [https://doi.org/10.1016/0008-8846\(96\)00134-2](https://doi.org/10.1016/0008-8846(96)00134-2).
- [8] Z.P. Bazant, S. Sener, J.K. Kim, Effect of cracking on drying permeability and diffusivity of concrete, *Vol. Acids Mater. J.* 84 (5) (1987) 351–357.
- [9] V. Picandet, A. Khelidj, H. Bellegou, Crack effects on gas and water permeability of concretes, *Cem. Concr. Res.* 39 (6) (2009) 537–547, <https://doi.org/10.1016/j.cemconres.2009.03.009>.
- [10] P.D. Tennis, H.M. Jennings, A model for two types of calcium silicate hydrate in the microstructure of Portland cement pastes, *Cem. Concr. Res.* 30 (6) (2000) 855–863, [https://doi.org/10.1016/S0008-8846\(00\)00257-X](https://doi.org/10.1016/S0008-8846(00)00257-X).
- [11] Z.P. Bazant, A. Steffens, Mathematical model for kinetics of alkali-silica reaction in concrete, *Cem. Concr. Res.* 30 (3) (2000) 419–428, [https://doi.org/10.1016/S0008-8846\(99\)00270-7](https://doi.org/10.1016/S0008-8846(99)00270-7).
- [12] F. Rajabipour, E. Giannini, C. Dunant, J.H. Ideker, M.D.A. Thomas, Alkali-silica reaction: current understanding of the reaction mechanisms and the knowledge gaps, *Cem. Concr. Res.* 76 (2015) 130–146, <https://doi.org/10.1016/j.cemconres.2015.05.024>.

- [13] A. Pichelin, M. Carcassès, F. Cassagnabère, S. Multon, G. Nahas, Sustainability, transfer and containment properties of concrete subject to delayed ettringite formation (DEF), *Cem. Concr. Compos.* 113 (2020) 103738, <https://doi.org/10.1016/j.cemconcomp.2020.103738>.
- [14] X. Brunetaud, L. Divet, D. Damidot, Impact of unrestrained Delayed Ettringite Formation-induced expansion on concrete mechanical properties, *Cem. Concr. Res.* 38 (11) (2008) 1343–1348, <https://doi.org/10.1016/j.cemconres.2008.05.005>.
- [15] Z. Zhang, J. Olek, S. Diamond, Studies on delayed ettringite formation in early-age, heat-cured mortars I. Expansion measurements, changes in dynamic modulus of elasticity, and weight gains, *Cem. Concr. Res.* 32 (11) (2002) 1729–1736.
- [16] D.M.M. Selman A.M. Ali, The Effect of Alkalies on The Properties of Portland Cement.
- [17] L. Huang, P. Yan, Effect of alkali content in cement on its hydration kinetics and mechanical properties, *Constr. Build. Mater.* 228 (2019) 116833, <https://doi.org/10.1016/j.conbuildmat.2019.116833>.
- [18] I. Odler, R. Wonnemann, Effect of alkalies on portland cement hydration II. Alkalies present in form of sulphates, *Cem. Concr. Res.* 13 (6) (1983) 771–777, [https://doi.org/10.1016/0008-8846\(83\)90078-9](https://doi.org/10.1016/0008-8846(83)90078-9).
- [19] I. Jawed, J. Skalny, Alkalies in cement: a review, *Cem. Concr. Res.* 8 (1) (1978) 37–51, [https://doi.org/10.1016/0008-8846\(78\)90056-X](https://doi.org/10.1016/0008-8846(78)90056-X).
- [20] N. Smaoui, M.A. Bérubé, B. Fournier, B. Bissonnette, B. Durand, Effects of alkali addition on the mechanical properties and durability of concrete, *Cem. Concr. Res.* 35 (2) (2005) 203–212, <https://doi.org/10.1016/j.cemconres.2004.05.007>.
- [21] A. Mohammadi, E. Ghiasvand, M. Nili, Relation between mechanical properties of concrete and alkali-silica reaction (ASR); a review, *Constr. Build. Mater.* 258 (2020) 119567, <https://doi.org/10.1016/j.conbuildmat.2020.119567>.
- [22] C.-M. Aldea, S.P. Shah, A. Karr, Effect of cracking on water and chloride permeability of concrete, *J. Mater. Civ. Eng.* 11 (3) (1999) 181–187, [https://doi.org/10.1061/\(ASCE\)0899-1561\(1999\)11:3\(181\)](https://doi.org/10.1061/(ASCE)0899-1561(1999)11:3(181)).
- [23] C.-M. Aldea, S.P. Shah, A. Karr, Permeability of cracked concrete, *Mater. Struct.* 32 (5) (1999) 370–376, <https://doi.org/10.1007/BF02479629>.
- [24] M. Choinska, A. Khehidj, G. Chatzigeorgiou, G. Pijaudier-Cabot, Effects and interactions of temperature and stress-level related damage on permeability of concrete, *Cem. Concr. Res.* 37 (1) (2007) 79–88, <https://doi.org/10.1016/j.cemconres.2006.09.015>.
- [25] G. Pijaudier-Cabot, F. Dufour, M. Choinska, Permeability due to the increase of damage in concrete: from diffuse to localized damage distributions, *J. Eng. Mech.* 135 (9) (2009) 1022–1028, [https://doi.org/10.1061/\(ASCE\)EM.1943-7889.0000016](https://doi.org/10.1061/(ASCE)EM.1943-7889.0000016).
- [26] G. Rastello, C. Boulay, S. Dal Pont, J.L. Tailhan, P. Rossi, Real-time water permeability evolution of a localized crack in concrete under loading, *Cem. Concr. Res.* 56 (2014) 20–28, <https://doi.org/10.1016/j.cemconres.2013.09.010>.
- [27] P. Rossi, Determination of the apparent gas permeability in a macrocracked concrete, *Engineering* 17 (2022) 93–98, <https://doi.org/10.1016/j.eng.2020.11.008>.
- [28] S. Rahal, A. Sellier, J. Verdier, Modelling of change in permeability induced by dilatancy for brittle geomaterials, *Constr. Build. Mater.* 125 (2016) 613–624, <https://doi.org/10.1016/j.conbuildmat.2016.08.002>.
- [29] J. Lindgård, E.J. Sellevold, M.D.A. Thomas, B. Pedersen, H. Justnes, T.F. Rønning, Alkali-silica reaction (ASR)—performance testing: Influence of specimen pretreatment, exposure conditions and prism size on concrete porosity, moisture state and transport properties, *Cem. Concr. Res.* 53 (2013) 145–167, <https://doi.org/10.1016/j.cemconres.2013.05.020>.
- [30] M. Al Shamaa, S. Lavaud, L. Divet, G. Nahas, J.M. Torrenti, Coupling between mechanical and transfer properties and expansion due to DEF in a concrete of a nuclear power plant, *Nucl. Eng. Des.* 266 (2014) 70–77, <https://doi.org/10.1016/j.nucengdes.2013.10.014>.
- [31] M. Al Shamaa, S. Lavaud, L. Divet, G. Nahas, J.M. Torrenti, Influence of relative humidity on delayed ettringite formation, *Cem. Concr. Compos.* 58 (2015) 14–22, <https://doi.org/10.1016/j.cemconcomp.2014.12.013>.
- [32] C. Zhao, M. Lei, C. Jia, C. Wu, Z. Yang, Y. Shi, Influence mechanism of initial mechanical damage on concrete permeability and tunnel lining leakage, *Eng. Fract. Mech.* 310 (2024) 110531, <https://doi.org/10.1016/j.engfracmech.2024.110531>.
- [33] D. Józwiak-Niedźwiedzka, M. Choinska Colombel, A. Brachaczek, M. Dąbrowski, J. Osko, M. Kuć, Gas permeability and gamma ray shielding properties of concrete for nuclear applications, *Nucl. Eng. Des.* 429 (2024) 113616, <https://doi.org/10.1016/j.nucengdes.2024.113616>.
- [34] Z. Long, et al., Effects of aggregates and fibers on the strength and permeability of concrete exposed to low vacuum environment, *J. Build. Eng.* 97 (2024) 110902, <https://doi.org/10.1016/j.jobbe.2024.110902>.
- [35] H. Zhang, B. Li, J. Shi, Y. Lu, P. Xu, Framework structure design based on porous permeable concrete material in expressway tunnel drainage system, *Desalin. Water Treat.* 317 (2024) 100308, <https://doi.org/10.1016/j.dwt.2024.100308>.
- [36] L. Charpin, et al., Predicting leakage of the VERCORS mock-up and concrete containment buildings - a digital twin approach, *Acta Polytech. CTU Proc.* 33 (2022) 78–84, <https://doi.org/10.14311/APP.2022.33.0078>.
- [37] Stark, D., The moisture condition of field concrete exhibiting alkali-silica reactivity, *Durability of Concrete*, p. G.M. IDORN International Symposium (pp. 973–987), 1992.
- [38] M. Abdou Ibro, J. Verdier, S. Geoffroy, H. Cagnon, X. Bourbon, Prediction of moisture transfer in cement-based materials: Use of a porous network model to access transfer parameters, *Cem. Concr. Res.* 142 (2021) 106310, <https://doi.org/10.1016/j.cemconres.2020.106310>.
- [39] N.R. Joshi, A. Matsumoto, S. Asamoto, T. Miura, Y. Kawabata, Investigation of the mechanical behaviour of concrete with severe delayed ettringite formation expansion focusing on internal damage propagation under various compressive loading patterns, *Cem. Concr. Compos.* 128 (2022) 104433, <https://doi.org/10.1016/j.cemconcomp.2022.104433>.
- [40] J. Jabbour, A. Darquennes, L. Divet, R. Bennacer, J.-M. Torrenti, G. Nahas, New experimental approach to accelerate the development of internal swelling reactions (ISR) in massive concrete structures, *Constr. Build. Mater.* 313 (2021) 125388, <https://doi.org/10.1016/j.conbuildmat.2021.125388>.
- [41] L.F.M. Sanchez, T. Drimalas, B. Fournier, Assessing condition of concrete affected by internal swelling reactions (ISR) through the Damage Rating Index (DRI), *Cement* 1-2 (2020) 100001, <https://doi.org/10.1016/j.cement.2020.100001>.
- [42] J. Jabbour, Méthodes d'essais de vieillissement accéléré des bétons à l'échelle des ouvrages, vol. 35, no 1, 2017.
- [43] M.H. Shehata, M.D.A. Thomas, The effect of fly ash composition on the expansion of concrete due to alkali-silica reaction, *Cem. Concr. Res.* 30 (7) (2000) 1063–1072, [https://doi.org/10.1016/S0008-8846\(00\)00283-0](https://doi.org/10.1016/S0008-8846(00)00283-0).
- [44] A.L. Roux J.S. Guedon-Dubied, The French preventive approach to AAR compared to experience. In Proceedings of the 10th International Conference on Alkali-Aggregate Reaction in Concrete (pp. 201–207). Melbourne, Australia.
- [45] X.X. Gao, M. Cyr, S. Multon, A. Sellier, A comparison of methods for chemical assessment of reactive silica in concrete aggregates by selective dissolution, *Cem. Concr. Compos.* 37 (2013) 82–94, <https://doi.org/10.1016/j.cemconcomp.2012.12.002>.
- [46] Réactivité d'un béton vis-à-vis d'une réaction sulfatique interne: essai de performance, Laboratoire central des ponts et chaussées, Paris, 2007.
- [47] M.Pascal Fasseu, Paris: Laboratoire des ponts et chaussées, 1997, Alcali-réaction du béton-Essai d'expansion résiduelle sur béton durci-Méthode d'essai n°44.
- [48] S. Poyet, et al., Influence of water on alkali-silica reaction: experimental study and numerical simulations, *J. Mater. Civ. Eng.* 18 (4) (2006) 588–596, [https://doi.org/10.1061/\(ASCE\)0899-1561\(2006\)18:4\(588\)](https://doi.org/10.1061/(ASCE)0899-1561(2006)18:4(588)).
- [49] S. Poyet, et al., Chemical modelling of Alkali Silica reaction: Influence of the reactive aggregate size distribution, *Mater. Struct.* 40 (2) (2007) 229–239, <https://doi.org/10.1617/s11527-006-9139-3>.
- [50] B. Kchakech. Étude de l'influence de l'échauffement subi par un béton sur le risque d'expansions associées à la Réaction Sulfatique Interne, Université Paris-Est, 2015. Pdd thesis, in French.
- [51] C. Famy, K.L. Scrivener, A. Atkinson, A.R. Brough, Influence of the storage conditions on the dimensional changes of heat-cured mortars, *Cem. Concr. Res.* 31 (5) (2001) 795–803, [https://doi.org/10.1016/S0008-8846\(01\)00480-X](https://doi.org/10.1016/S0008-8846(01)00480-X).
- [52] AFNOR, Béton — Essai pour béton durci — Essai de porosité et de masse volumique-NF P 18-459, août 2022.
- [53] Groupe de travail Durabilité des bétons (France), Jean-Pierre Ollivier, Laboratoire Matériaux et durabilité des constructions (Toulouse), Compte-rendu des journées techniques AFPC-AFREM, Durabilité des bétons: méthodes recommandées pour la mesure des grandeurs associées à la durabilité: 11 et 12 décembre 1997, Toulouse.

- [54] ISO/TC 24/SC 4/WG 3, Evaluation de la distribution de taille des pores et la porosité des matériaux solides par porosimétrie à mercure et l'adsorption des gaz - Partie 1: Porosimétrie à mercure-ISO 15901-1:2016, 1 avril 2016.
- [55] V. Baroghel-Bouny, Water vapour sorption experiments on hardened cementitious materials, *Cem. Concr. Res.* 37 (3) (2007) 414–437, <https://doi.org/10.1016/j.cemconres.2006.11.019>.
- [56] V. Baroghel-Bouny, Water vapour sorption experiments on hardened cementitious materials. Part II: Essential tool for assessment of transport properties and for durability prediction, *Cem. Concr. Res.* 37 (3) (2007) 438–454, <https://doi.org/10.1016/j.cemconres.2006.11.017>.
- [57] H. Cagnon, T. Vidal, A. Sellier, C. Soula, X. Bourbon, G. Camps, Effects of water and temperature variations on deformation of limestone aggregates, cement paste, mortar and High Performance Concrete (HPC), *Cem. Concr. Compos.* 71 (2016) 131–143, <https://doi.org/10.1016/j.cemconcomp.2016.05.013>.
- [58] H. Zhu, Y. Hu, Q. Li, R. Ma, Restrained cracking failure behavior of concrete due to temperature and shrinkage, *Constr. Build. Mater.* 244 (2020) 118318, <https://doi.org/10.1016/j.conbuildmat.2020.118318>.
- [59] Zdenek P. Bazant, Werapol Thonguthai, Pore pressure and drying of concrete at high temperature, *Civil and Environmental Engineering*, p. 21.
- [60] H. Sogbossi, J. Verdier, S. Multon, Permeability and damage of partially saturated concrete exposed to elevated temperature, *Cem. Concr. Compos.* 109 (2020) 103563, <https://doi.org/10.1016/j.cemconcomp.2020.103563>.
- [61] M. Carcasses A. Abbas, An optimised preconditioning procedure for gas permeability measurement, p. 6.
- [62] D.R. Gardner, R.J. Lark, B. Barr, Effect of conditioning temperature on the strength and permeability of normal- and high-strength concrete, *Cem. Concr. Res.* 35 (7) (2005) 1400–1406, <https://doi.org/10.1016/j.cemconres.2004.08.012>.
- [63] D.R. Gardner, A.D. Jefferson, R.J. Lark, An experimental, numerical and analytical investigation of gas flow characteristics in concrete, *Cem. Concr. Res.* 38 (3) (2008) 360–367, <https://doi.org/10.1016/j.cemconres.2007.10.001>.
- [64] Z. Wu, H.S. Wong, N.R. Buenfeld, Influence of drying-induced microcracking and related size effects on mass transport properties of concrete, *Cem. Concr. Res.* 68 (2015) 35–48, <https://doi.org/10.1016/j.cemconres.2014.10.018>.
- [65] AFNOR, Bétons - Essai de perméabilité aux gaz sur béton durci- XP P18-463, 13 décembre 2023.
- [66] E.R. Giannini, L.F.M. Sanchez, A. Tuinukuafe, K.J. Folliard, Characterization of concrete affected by delayed ettringite formation using the stiffness damage test, *Constr. Build. Mater.* 162 (2018) 253–264, <https://doi.org/10.1016/j.conbuildmat.2017.12.012>.
- [67] Joe Maalouf, Hugo Cagnon, Jérôme Verdier, Jacques Jabbour & Stéphane Multon, Evolution of Air Permeability of Concrete due to Expansion Caused by Internal Swelling Reactions (ISR), p. pp 796-808.
- [68] J.J. Kolek, The determination of the permeability of concrete to oxygen by the Cembureau method—a recommendation, *Mater. Struct.* 22 (3) (1989) 225–230, <https://doi.org/10.1007/BF02472192>.
- [69] H. Sogbossi, J. Verdier, S. Multon, New approach for the measurement of gas permeability and porosity accessible to gas in vacuum and under pressure, *Cem. Concr. Compos.* 103 (2019) 59–70, <https://doi.org/10.1016/j.cemconcomp.2019.04.032>.
- [70] C. Larive, A. Laplaud, M. Joly, Behaviour of AAR-affected concrete, Experimental data.
- [71] G. Giaccio, M.C. Torrijos, C. Milanese, R. Zerbinio, Alkali-silica reaction in plain and fibre concretes in field conditions, *Mater. Struct.* 52 (2) (2019) 31, <https://doi.org/10.1617/s11527-019-1332-2>.
- [72] L.F.M. Sanchez, B. Fournier, M. Jolin, J. Duchesne, Reliable quantification of AAR damage through assessment of the Damage Rating Index (DRI), *Cem. Concr. Res.* 67 (2015) 74–92, <https://doi.org/10.1016/j.cemconres.2014.08.002>.
- [73] X. Brunetaud, R. Linder, L. Divet, D. Duragrin, D. Damidot, Effect of curing conditions and concrete mix design on the expansion generated by delayed ettringite formation, *Mater. Struct.* 40 (6) (2007) 567–578, <https://doi.org/10.1617/s11527-006-9163-3>.
- [74] P.E. Grattan-Bellew, J.J. Beaudoin, V.-G. Vallée, Effect of aggregate particle size and composition on expansion of mortar bars due to delayed ettringite formation, *Cem. Concr. Res.* 28 (8) (1998) 1147–1156, [https://doi.org/10.1016/S0008-8846\(98\)00084-2](https://doi.org/10.1016/S0008-8846(98)00084-2).
- [75] B. Fournier M.-A. Bérubé, Alkali-aggregate reaction in concrete: a review of basic concepts and engineering implications, vol. 27, 2000.
- [76] S. Multon, A. Sellier, Expansion modelling based on cracking induced by the formation of new phases in concrete, *Int. J. Solids Struct.* 160 (2019) 293–306, <https://doi.org/10.1016/j.ijsolstr.2018.11.001>.
- [77] R. Yang, C.D. Lawrence, J.H. Sharp, Effect of type of aggregate on delayed ettringite formation, *Adv. Cem. Res.* 11 (3) (1999) 119–132, <https://doi.org/10.1680/adcr.1999.11.3.119>.
- [78] B. Lothenbach, F. Winnefeld, C. Alder, E. Wieland, P. Lunk, Effect of temperature on the pore solution, microstructure and hydration products of Portland cement pastes, *Cem. Concr. Res.* 37 (4) (2007) 483–491, <https://doi.org/10.1016/j.cemconres.2006.11.016>.
- [79] J.J. Thomas, D. Rothstein, H.M. Jennings, B.J. Christensen, Effect of hydration temperature on the solubility behavior of Ca-, S-, Al-, and Si-bearing solid phases in Portland cement pastes, *Cem. Concr. Res.* 33 (12) (2003) 2037–2047, [https://doi.org/10.1016/S0008-8846\(03\)00224-2](https://doi.org/10.1016/S0008-8846(03)00224-2).
- [80] H.F.W. Taylor. *Cement chemistry*, 2nd ed, T. Telford, London, 1997.
- [81] P. Padilla-Encinas, L. Fernández-Carrasco, A. Palomo, A. Fernández-Jiménez, Effect of alkalinity on early-age hydration in calcium sulfoaluminate clinker, *Cem. Concr. Res.* 155 (2022) 106781, <https://doi.org/10.1016/j.cemconres.2022.106781>.
- [82] S. Bahafid, S. Ghabezloo, M. Duc, P. Faure, J. Sulem, Effect of the hydration temperature on the microstructure of Class G cement: C-S-H composition and density, *Cem. Concr. Res.* 95 (2017) 270–281, <https://doi.org/10.1016/j.cemconres.2017.02.008>.
- [83] L. Wang, H.Q. Yang, S.H. Zhou, E. Chen, S.W. Tang, Hydration, mechanical property and C-S-H structure of early-strength low-heat cement-based materials, *Mater. Lett.* 217 (2018) 151–154, <https://doi.org/10.1016/j.matlet.2018.01.077>.
- [84] S. Multon, F. Toutlemonde, Effect of moisture conditions and transfers on alkali silica reaction damaged structures, *Cem. Concr. Res.* 40 (6) (2010) 924–934, <https://doi.org/10.1016/j.cemconres.2010.01.011>.
- [85] A. Abbas, M. Carcasses, J.-P. Ollivier, Gas permeability of concrete in relation to its degree of saturation, *Mater. Struct.* 32 (1) (1999) 3–8, <https://doi.org/10.1007/BF02480405>.
- [86] T.L.P. Hang, J. Verdier, T. Vidal, G. Camps, X. Bourbon, Mechanical and transfer properties of low-pH concretes in view of classical HPC substitution in confinement structures, *Eur. J. Environ. Civ. Eng.* 23 (6) (2019) 657–674, <https://doi.org/10.1080/19648189.2017.1304274>.
- [87] J. Cai, E. Perfect, C.-L. Cheng, X. Hu, Generalized modeling of spontaneous imbibition based on hagen-poiseuille flow in tortuous capillaries with variably shaped apertures, *Langmuir* 30 (18) (2014) 5142–5151, <https://doi.org/10.1021/la5007204>.